

# CO rotational line emission from a dense knot in Cas A

## Evidence for active post-reverse-shock chemistry

Sofia H. J. Wallström<sup>1</sup>, Chiara Biscaro<sup>2</sup>, Francisco Salgado<sup>3</sup>, John H. Black<sup>1</sup>, Isabelle Cherchneff<sup>2</sup>, Sébastien Muller<sup>4</sup>, Olivier Berné<sup>5,6</sup>, Jeonghee Rho<sup>7,8</sup>, and Alexander G. G. M. Tielens<sup>3</sup>

<sup>1</sup> Department of Earth and Space Sciences, Chalmers University of Technology, SE-43992 Onsala, Sweden

<sup>2</sup> Department Physik, Universität Basel, CH-4056 Basel, Switzerland

<sup>3</sup> Leiden Observatory, Leiden University, P.O. Box 9513, NL-2300 RA, The Netherlands

<sup>4</sup> Onsala Space Observatory, Chalmers University of Technology, SE-43992 Onsala, Sweden

<sup>5</sup> Université de Toulouse, UPS-OMP, IRAP, 31028 Toulouse, France

<sup>6</sup> CNRS; IRAP; 9 Av. Colonel Roche, BP 44346, F-31028 Toulouse cedex 4, France

<sup>7</sup> SETI Institute, 189 N. Bernardo Ave, Mountain View, CA 94043

<sup>8</sup> Stratospheric Observatory for Infrared Astronomy, NASA Ames Research Center, MS 211-3, Moffett Field, CA 94035, USA

Received / Accepted

### ABSTRACT

We report a *Herschel*\* detection of high-J rotational CO lines from a dense knot in the supernova remnant Cas A. Based on a combined analysis of these rotational lines, and previously observed ro-vibrational CO lines, we find the gas to be warm (two components at  $\sim 400$  and  $2000$  K) and dense ( $10^{6-7}$  cm $^{-3}$ ), with a CO column density of  $\sim 5 \times 10^{17}$  cm $^{-2}$ . This, along with the broad line widths ( $\sim 400$  km s $^{-1}$ ), suggests that the CO emission originates in the post-shock region of the reverse shock. As the passage of the reverse shock dissociates any existing molecules, the CO has most likely reformed in the last few years, in the post-shock gas. The CO cooling time is comparable to the CO formation time, so possible heating sources (UV photons from the shock front, X-rays, electron conduction) to maintain the large column density of warm CO are discussed.

**Key words.** ISM: supernova remnants, ISM: individual objects: Cassiopeia A, ISM: molecules

## 1. Introduction

Stars with masses ranging from 8 to 30  $M_{\odot}$  have lifetimes of some  $10^7$  years (Woosley et al., 2002) before exploding as Type II supernovae (SNe), enriching their local environments on a short timescale. Dust grains and molecules are produced in the ejected material (ejecta), despite the harsh physical conditions. Emission from CO and SiO molecules has been observed at infrared (IR) wavelengths in SN1987A some hundred days after the SN explosion (Danziger et al., 1987; Lucy et al., 1989; Roche et al., 1991), and in several other SNe (Kotak et al., 2005, 2006, 2009). These observations demonstrate that a rapid and efficient chemistry develops in the ejecta, and that molecular formation is a common occurrence in SNe (Lepp et al., 1990; Cherchneff & Sarangi, 2011). CO and SiO have been observed in the ejecta of SN1987A (Kamenetzky et al., 2013), demonstrating that these molecules have survived up to 25 years after the SN explosion.

SNe are prime contenders for explaining the large dust masses in the early universe, inferred from the reddening of background quasars and Lyman- $\alpha$  systems at high redshift (Pei et al., 1991; Pettini et al., 1994; Bertoldi et al., 2003), as efficient dust formation on short timescales is required.

However, IR observations of SNe  $\sim 400$  days post-explosion show dust masses ranging between  $10^{-5}$  and  $10^{-2}$   $M_{\odot}$  (e.g., Lucy et al., 1989; Sugerman et al., 2006; Szalai & Vinkó, 2013), at least an order of magnitude too little to explain the observed high-z dust (Dwek et al., 2008). Larger dust masses have been observed in supernova remnants (SNRs), for example  $\sim 0.7$   $M_{\odot}$  of cool dust in the young remnant of SN1987A (Matsuura et al., 2011). Observations of the SNR Cas A imply  $\sim 0.025$   $M_{\odot}$  of warm dust (Rho et al., 2008), and  $\sim 0.075$   $M_{\odot}$  of cool dust (Barlow et al., 2010). However, these dust masses do not necessarily represent the net SN dust yields into the ISM, as the passage of a reverse shock might reprocess the dust grains.

When a SN explosion shock wave has swept up enough circumstellar and interstellar matter, a reverse shock forms and travels inwards, decelerating and reprocessing the ejecta (Chevalier, 1977). At the shock front the ejecta will be heated to  $>10^6$  K, sputtering dust and dissociating molecules. However, the shock can be attenuated in dense knots in the ejecta, mitigating its destructive effects there.

The 330-year-old SNR Cas A ( $D=3.4$  kpc) is the perfect laboratory for studying the effects of the reverse shock, as it is just beginning to reprocess the ejecta. Ro-vibrational CO emission has been detected in Cas A (Rho et al., 2009, 2012), in several ( $\sim 20$ ) small ( $<0.8''$ ) knots coincident with the reverse shock. Such knots are reminiscent of the fast-moving knots (FMKs) seen in the optical (Fesen, 2001). In

\* *Herschel* is an ESA space observatory with science instruments provided by European-led Principal Investigator consortia and with important participation from NASA.

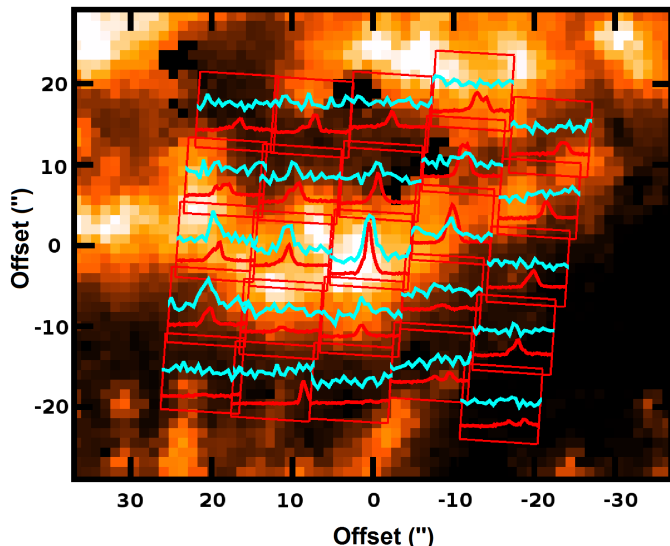


**Fig. 1.** The PACS footprint, centered on RA 23:23:24.9 Dec +58:50:03.3, showing the spectra of CO  $J=23-22$  in blue and [O III]  $88\mu\text{m}$  in red, overlaid on a Spitzer/IRAC image of CO vibrational emission in Cas A.

order to determine the chemical and physical conditions in these knots, we used the Herschel PACS instrument to observe several high- $J$  rotational CO lines towards the brightest CO knot in the remnant.

## 2. Observations

The Photodetector Array Camera and Spectrometer (PACS; Poglitsch et al., 2010) aboard the Herschel Space Observatory (Pilbratt et al., 2010) was used on 2012 June 11, to observe a single pointing in the northwest of Cas A (Fig. 1). PACS consists of a  $5\times 5$  array of spatial pixels (spaxels), each  $9.4''\times 9.4''$  in size. We selected seven CO rotational transitions, between  $J_{up}=14$  and 38, for even coverage of the CO ladder in the PACS spectral range. The observations were done using short range spectroscopy scans with high spectral resolution ( $R=1000-2700$ ,  $\sim 100-300\text{ km s}^{-1}$ ). The [O III]  $88\mu\text{m}$  transition was observed within the covered spectral range. Observations were done in chopping/nodding mode with a chop throw of  $6'$  to the north and south, well off the remnant.

The data were processed using the standard range scan reduction pipeline, implemented in HIPE version 9.0.0 (Ott, 2010). The CO  $J=38-37$  spectrum was marred by an artifact and thus discarded. A first degree polynomial baseline was fit from line-free channels and subtracted. The final spectra correspond to the central spaxel after applying the standard PACS point source correction, to correct for flux spill-over into adjacent spaxels. PACS has an absolute flux accuracy of  $\sim 10\%$  (PACS Observer’s Manual).

## 3. Results

All the targeted CO lines are detected in the central PACS spaxel. The line profiles extracted from the central spaxel (Fig. 2) were fit with gaussians (Table 1). The lines have an average radial velocity of  $-2740\text{ km s}^{-1}$ , consistent with

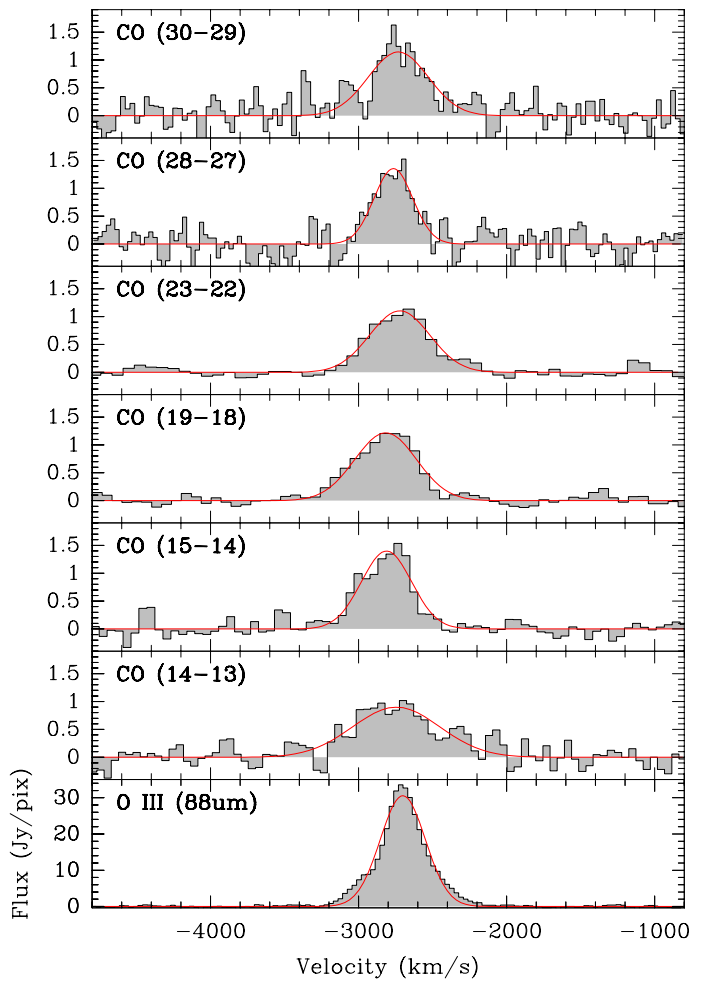


**Fig. 2.** CO, and O III, emission lines in velocity (LSR), with Gaussian fits, extracted from the central PACS spaxel. Note that the flux density scale is different for the O III line.

the velocity of the IR knot n2 (Rho et al., 2012, close to our target position), and are broad, with a deconvolved FWHM  $\sim 400\text{ km s}^{-1}$ .

The integrated CO line fluxes were used to create a rotational diagram (Goldsmith & Langer, 1999), as shown in Fig. 3. We adopt a source diameter of  $0.5''$  (much smaller than the spaxel size), consistent with the  $0.8''$  upper limit on the near-IR ro-vibrational CO source size (Rho et al., 2009) and optical observations of FMKs (Fesen, 2001). Assuming local thermal equilibrium (LTE) conditions, we derive a column density of  $N_{CO}=(4.1\pm 0.3)\times 10^{17}\text{ cm}^{-2}$  and a rotation temperature of  $T_{rot}=560\pm 20\text{ K}$ . This corresponds to a CO mass of  $\sim 5\times 10^{-6}\text{ M}_{\odot}$  for the knot, which is independent of the assumed knot size, as  $N_{CO}$  is inversely proportional to the knot size squared.

In the spectra of the full PACS footprint (Fig. 1) we see that the central spaxel emission has spilled over into the adjacent spaxels, because the point spread function is larger than the spaxel size. There is also some additional CO emission at the eastern edge of the footprint. This is most likely indicative of a second knot, rather than extended CO emission, given the IR and optical evidence for a multitude of small, dense knots. Due to the increased uncertainty at the edge of the PACS footprint, and the smaller CO fluxes,

**Table 1.** Data on the CO and [O III] lines extracted from the central spaxel.  $v_0$  is the radial velocity of the line, and  $\delta v$  the velocity full width at half maximum. Errors are given in parentheses.

Line	$\lambda$ $\mu\text{m}$	$v_0$ $\text{km s}^{-1}$	$\delta v$ $\text{km s}^{-1}$	$\int \text{Flux } dv$ $10^{-18} \text{ W m}^{-2}$
CO (14-13)	186.00	-2882(370)	661(63)	35(2)
CO (15-14)	173.63	-2814(362)	336(24)	34(2)
CO (19-18)	137.20	-2814(336)	409(19)	46(2)
CO (23-22)	113.46	-2716(309)	372(19)	50(2)
CO (28-27)	93.35	-2765(105)	292(32)	48(4)
CO (30-29)	87.19	-2733(470)	418(46)	64(6)
[O III]	88.36	-2701(100)	341(7)	1310(20)

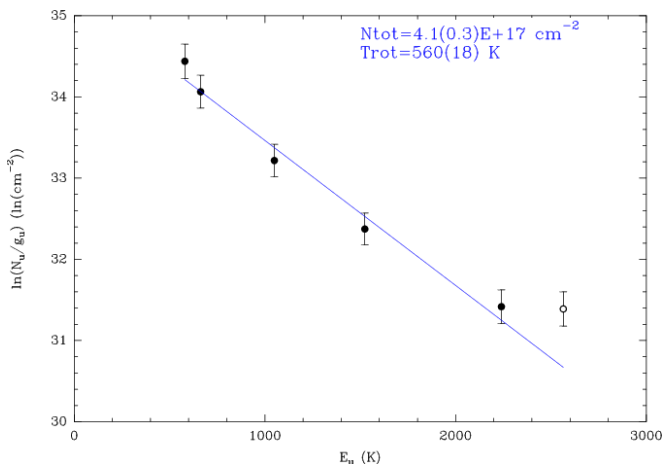


**Fig. 3.** CO excitation diagram, plotting  $\ln(N_u/g_u)$  vs.  $E_u$ . The column density,  $N_{tot}$ , and rotation temperature,  $T_{rot}$ , and their uncertainties, were calculated by Monte Carlo method, excluding the last point; the blue line corresponds to those best-fit parameters.

we do not attempt to analyze this emission. In contrast to the CO, the emission of the [O III] line is extended over the PACS footprint, which might be explained by its lower critical density as compared with the high-J CO lines.

#### 4. Discussion

To further investigate the physical conditions in the knot we analyse the CO excitation with the non-LTE radiative transfer code RADEX (van der Tak et al., 2007), assuming a uniform emitting region (i.e. constant density, temperature, and abundance). In order to fit all our rotational lines, as well as the previously reported ro-vibrational emission from the same region (Rho et al., 2009, 2012), multiple temperature components are required: a  $\sim 400$  K component, and an additional  $\sim 2000$  K component, containing about 15% of the CO, to explain the ro-vibrational fluxes (shown in Fig. 4). This hot component also contributes substantially to the high-J rotational lines. The multiple temperature components are suggestive of the structure of a post-shock cooling zone (Borkowski & Shull, 1990).

The non-LTE analysis yields  $N_{CO} \sim 5 \times 10^{17} \text{ cm}^{-2}$ , comparable to the rotation diagram result. The required

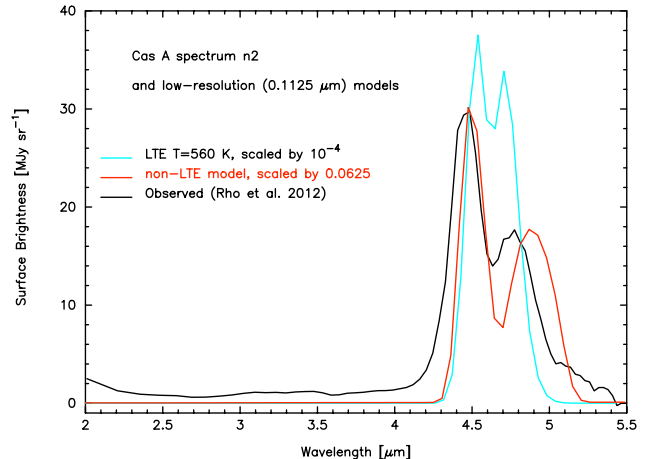


**Fig. 4.** The mid-IR AKARI spectrum reported by (Rho et al., 2012) for knot n2 in Cas A is compared with models that have been convolved to the same resolution,  $0.1125 \mu\text{m}$ . The black curve is the observed spectrum. The red curve is the computed spectrum for the same two-component non-LTE model that best describes the fluxes of the CO rotational lines, but scaled in intensity by a factor  $1/16$ . The cyan curve represents the vibrational emission expected in strict LTE for the column density and temperature derived from the rotation diagram in Figure 3, but scaled down by a factor of  $10^{-4}$ . The computed spectra include more than 4000 vibration-rotation lines, each of which has a width of  $415 \text{ km s}^{-1}$ .

density of the main collision partner is  $\sim 10^6 \text{ cm}^{-3}$ . As the knot is expected to be oxygen-rich, with its strong [O III] emission and similarity to optical FMKs, we consider oxygen to be the main collision partner in this knot. However, collisional rates with CO have only been studied with  $\text{H}/\text{H}_2$  and  $\text{H}_2\text{O}$  as collision partners. Hence, these rates have been used as proxies for the unknown  $\text{O} + \text{CO}$  collisional rates. The derived density differs by an order of magnitude depending on the chosen collision partner. On the other hand, the critical densities of the observed CO lines are  $\sim 10^{6-7} \text{ cm}^{-3}$ , constraining the gas density to be fairly high. The RADEX analysis indicates that the observed CO lines are optically thin ( $\tau < 10^{-2}$ ). Overall, the non-LTE analysis results are consistent with the simple rotational diagram analysis.

The high temperature and density of the CO, along with the broad ( $\sim 400 \text{ km s}^{-1}$ ) lines, suggests that the CO emission originates in a dense knot in the post-shock region of the reverse shock. In a dense knot, the reverse shock is attenuated due to energy conservation. Following Docenko & Sunyaev (2010), a  $2000 \text{ km s}^{-1}$  reverse shock will be slowed to  $200 \text{ km s}^{-1}$  when crossing a knot 100 times denser than the interclump medium. For a  $200 \text{ km s}^{-1}$  shock, the gas temperature at the shock front reaches some  $10^7 \text{ K}$  and any pre-existing molecules, including CO, will be destroyed. However, ongoing chemical modeling suggests that, under the observed post-shock conditions, CO will reform on a

timescale  $t_{CO} \sim 100$  days, through radiative association reactions (Biscaro & Cherchneff, in prep.).

Shock attenuation in dense knots also has implications for the survival of SN-produced dust. A slow shock may sputter  $< 50\%$  of the dust mass (Silvia et al., 2012), and the warm dense gas we see in the post-shock region is conducive to grain growth. Hence, some SN dust may survive the passage of the reverse shock in dense knots.

A minimum cooling flux,  $\Lambda_{min}$ , can be estimated from the energy radiated by the observed [O III] and CO lines in our knot. The [O III]  $88\ \mu\text{m}$  line provides  $\sim 1\ \text{erg cm}^{-2}\ \text{s}^{-1}$  of cooling, comparable to that of the total rotational CO line emission, giving  $\Lambda_{min} \sim 2\ \text{erg cm}^{-2}\ \text{s}^{-1}$ . Using a gas column density of  $5 \times 10^{19}\ \text{cm}^{-2}$ , as explained below, we can calculate an approximate gas cooling time ( $t_{cool} = N_{gas} k_B T / \Lambda_{min}$ ) of 70 days. This is comparable to the CO formation timescale  $t_{CO} \sim 100$  days, indicating that a constant heating flux of the order of  $\Lambda_{min}$  may be required to maintain the observed large column density of warm CO.

One obvious heat source is the shock front itself, which emits UV photons. For a flux of  $F_o = n_o \times v_s$  ( $n_o$ =oxygen density;  $v_s$ =shock velocity) oxygen atoms flowing into the shock, the total UV photon flux at the surface of the knot is  $30 F_o$  photons  $\text{cm}^{-2}\ \text{s}^{-1}$  (Borkowski & Shull, 1990, Table 11). With a typical photon energy of 20 eV, we thus derive a heating flux of  $\sim 2\ \text{erg cm}^{-2}\ \text{s}^{-1}$ , comparable to  $\Lambda_{min}$ . However, the penetration depth of the UV photons is only  $\sim 3 \times 10^{17}\ \text{cm}^{-2}$  (Borkowski & Shull, 1990), while the derived O III column density is  $\sim 10^{19}\ \text{cm}^{-2}$ . In addition,  $N_{CO} \sim 5 \times 10^{17}\ \text{cm}^{-2}$  implies a gas column density of at least  $5 \times 10^{19}\ \text{cm}^{-2}$ , as the pre-shock CO abundance in such a knot is expected to be  $\sim 10^{-2}$  (Sarangi & Cherchneff, 2013). Hence, the UV photons cannot penetrate the full gas column, and additional heating sources must be considered.

The reverse shock traveling through the tenuous inter-knot ejecta creates a hot plasma which will slowly cool through X-rays. Taking the average observed X-ray luminosity over the remnant,  $5.5 \times 10^{37}\ \text{erg s}^{-1}$  (Hartmann et al., 1997), with a typical photon energy of  $\sim 2\ \text{keV}$ , we get an X-ray heating flux of  $0.2\ \text{erg cm}^{-2}\ \text{s}^{-1}$  at the knot. While the keV photons could ionize and heat a much larger column density than the UV photons,  $\sim 3 \times 10^{19}\ \text{cm}^{-2}$ , the X-ray heating flux falls short of  $\Lambda_{min}$  by an order of magnitude.

Heat conduction from the inter-knot hot, tenuous plasma into the dense knot could provide another heating source. The classical expression for heat conduction by electrons gives  $Q = K(T) dT/dr$  where  $K(T)$  is approximately constant and about  $6 \times 10^{-7} \times T^{5/2}\ \text{erg s}^{-1}\ \text{K}^{-7/2}\ \text{cm}^{-1}$  (Tielens, 2005, p. 448–449). Setting the temperature gradient equal to  $T/\delta R$  with the temperature  $T=10^7\ \text{K}$  and the length scale  $\delta R$  given by the gas column density divided by the gas density,  $N/n = 5 \times 10^{13}\ \text{cm}$ , we find an energy flux of  $\sim 4 \times 10^4\ \text{erg cm}^{-2}\ \text{s}^{-1}$  which will be balanced by mass evaporation from the knot surface. The energy radiated away through the CO lines is then of little relevance for the energy budget. For the adopted parameters, the mean free path for electrons ( $\sim 10^{12}\ \text{cm}$ ) is small compared with the size scale for the temperature gradient ( $5 \times 10^{13}\ \text{cm}$ ), as required by the classical heat conduction expression. Though the heat flux conducted inwards by electrons may be limited somewhat by magnetic fields, still heat conduction may be key to maintaining the large column density of warm gas.

In conclusion, *Herschel* observations of rotational CO lines in a dense knot in Cas A indicate a large column density ( $N_{CO} \sim 5 \times 10^{17}\ \text{cm}^{-2}$ ) of warm (two components at  $\sim 400$  and  $2000\ \text{K}$ ) and dense ( $10^{6-7}\ \text{cm}^{-3}$ ) gas in the post-shock region of the reverse shock. The passage of the shock will dissociate any existing molecules and hence the CO has most likely been reformed recently, in the post-shock gas, providing evidence of an active chemistry in the post-reverse-shock region. The observed large column density of warm CO indicates that the cooling through CO (and ionic) lines is balanced by a constant heating flux. The diffuse X-ray flux is insufficient, and the UV photons from the shock front cannot penetrate the full gas column, so heat conduction by electrons may be required to maintain the temperature of the gas.

*Acknowledgements.* S.W. and C.B. thank the ESF EuroGENESIS programme for financial support through the CoDustMas network.

## References

- Aitken, D. K.; Smith, C. H.; James, S. D.; et al., 1988, MNRAS, 235, 19  
 Baade, W. & Minkowski, R., 1954, ApJ, 119, 206  
 Barlow, M. J.; Krause, O.; Swinyard, B. M.; et al., 2010, A&A, 518, 138  
 Beelen, A.; Cox, P.; Benford, D. J.; et al., 2006, ApJ, 642, 694  
 Bertoldi, F.; Carilli, C. L.; Cox, P.; et al., 2003, A&A, 406, 55  
 Borkowski, K. J. & Shull, M. J., 1990, ApJ, 348, 169  
 Chevalier, R., 1977, ARA&A 15, 175  
 Chevalier, R. A. & Kirshner, R. P., 1979, ApJ, 233, 154  
 Cherchneff, I. & Sarangi, A., 2011, IAU Symposium, 280, 22  
 Danziger, I. J.; Fosbury, R. A. E.; Alloin, D.; et al., 1987, A&A, 177, L13  
 Docenko, D. & Sunyaev, R.A., 2008, A&A, 484, 755  
 Docenko, D. & Sunyaev, R.A., 2010, A&A, 509, 59  
 Dwek, E.; Arendt, R. G.; Bouchet, P.; et al., 2008, ApJ, 676, 1029  
 Fesen, R. A., 2001, ApJS, 133, 161  
 Goldsmith, P. F. & Langer, W. D., 1999, ApJ, 517, 209  
 Hartmann, D. H.; Predehl, P.; Greiner, J.; et al., 1997, Nuclear Physics A, 621, 83  
 Hollenbach & McKee, 1989, ApJ, 342, 306  
 Kamenetzky, J.; McCray, R.; Indebetouw, R.; et al., 2013, ApJ, 773, 34  
 Kotak, R.; Meikle, P.; van Dyk, S. D.; et al., 2005, ApJ, 628, L123  
 Kotak, R.; Meikle, P.; Pozzo, M.; et al., 2006, ApJ, 651, L117  
 Kotak, R.; Meikle, W. P. S.; Farrah, D.; et al., 2009, ApJ, 704, 306  
 Krause, O.; Birkmann, S.; Usuda, T.; et al., 2008, Science, 320, 1195  
 Lepp, S.; Dalgarno, A., & McCray, R., 1990, ApJ, 358, 262  
 Lucy, L.B.; Danziger, I.J.; Gouiffes, C. & Bouchet, P., 1989, in G. Tenorio-Tagle, M. Moles & J. Melnick (eds.), IAU Colloq. 120 'Structure and Dynamics of the Interstellar Medium', p. 164  
 Matsuura, M.; Dwek, E.; Meixner, M.; et al., 2011, Science, 333, 1258  
 Nozawa, T.; Kozasa, T.; Habe, A.; et al., 2007, ApJ, 666, 955  
 Ott, S., 2010, ASP Conference Series, 434, 139  
 Pei, Y. C.; Fall, S. M. & Bechtold, J., 1991, ApJ, 378, 6  
 Pettini, M.; Smith, L. J.; Hunstead, R. W. & King, D. L., 1994, MNRAS, 394, 2266  
 Pilbratt, G.; Riedinger, J.; Passvogel, T.; et al., 2010, A&A, 518, L1  
 Poglitsch, A.; Waelkens, C.; Geis, N.; et al., 2010, A&A, 518, L2  
 Rho, J.; Kozasa, T.; Reach, W. T.; et al., 2008, ApJ, 673, 271  
 Rho, J.; Jarrett, T. H.; Reach, W. T.; et al., 2009, ApJ, 693, 39  
 Rho, J.; Onaka, T.; Cami, J. & Reach, W. T., 2012, ApJ, 747, 6  
 Roche, P. F., Aitken, D. K. & Smith, C. H., 1991, MNRAS, 252, 39  
 Sarangi A. & Cherchneff I., 2013, ApJ, in press  
 Silvia, D. W.; Smith, B. D. & Shull, J. M., 2012, ApJ, 748, 12  
 Smith, J. D. T.; Rudnick, L.; Delaney, T.; et al., 2009, ApJ, 693, 713  
 Sugerman, B. E. K.; Ercolano, B.; Barlow, M. J.; et al., 2006, Science, 313, 196  
 Sutherland, R. S. & Dopita, N. A., 1995, ApJ, 439, 381  
 Szalai, T. & Vinkó, J., 2013, A&A 549, A79  
 Thielemann, F.-K.; Nomoto, K. & Hashimoto, M., 1996, ApJ, 460, 408

- Tielens, A. G. G. M., 2005, *The Physics and Chemistry of the Interstellar Medium* (Cambridge University Press)
- van den Bergh, S. & Dodd, W. W., 1970, *ApJ*, 162, 485
- van der Tak, F. F. S.; Black, J. H.; Schier, F. L.; et al., 2007, *A&A*, 468, 627
- Woosley, S. E.; Heger, A. & Weaver, T. A., 2002, *RvMP*, 74, 1015